

General Synthesis of Di- $\mu$ -oxo Dimanganese Complexes as Functional Models for the Oxygen Evolving Complex of Photosystem II

Hongyu Chen, Ranitendranath Tagore, Siddhartha Das, Christopher Incarvito, J. W. Faller, Robert H. Crabtree,\* and Gary W. Brudvig\*

Department of Chemistry, Yale University, P.O. Box 208107, New Haven, Connecticut 06520-8107

Received June 17, 2005

A series of complexes with the formula  $[\text{Mn}^{\text{III/IV}}_2(\mu\text{-O})_2(\text{L})_2(\text{X})_2]^{3+}$  have been prepared in situ from  $\text{Mn}^{\text{II}}\text{LCl}_2$  precursors by a general preparative method ( $\text{L}$  = terpy, Cl-terpy, Br-terpy, Ph-terpy, tolyl-terpy, mesityl-terpy,  $t\text{Bu}_3$ -terpy, EtO-terpy, py-phen, dpys,  $\text{Me}_2\text{N}$ -terpy, or HO-terpy, and  $\text{X}$  = a labile ligand such as water, chloride, or sulfate). The parent complex, where  $\text{L}$  = terpy and  $\text{X}$  = water, is a functional model for the oxygen-evolving complex of photosystem II (Limburg, et al. *J. Am. Chem. Soc.* **2001**, 123, 423–430). Crystals of  $\text{Mn}^{\text{II}}(\text{dpys})\text{Cl}_2$ ,  $\text{Mn}^{\text{II}}(\text{Ph-terpy})\text{Cl}_2$ ,  $\text{Mn}^{\text{II}}(\text{mesityl-terpy})\text{Cl}_2$ , and an organic-soluble di- $\mu$ -oxo di-aqua dimanganese complex,  $[\text{Mn}^{\text{III/IV}}_2(\mu\text{-O})_2(\text{mesityl-terpy})_2(\text{OH}_2)_2](\text{NO}_3)_3$ , were obtained and characterized by X-ray crystallography. Solutions of the in situ-formed di- $\mu$ -oxo dimanganese complexes were characterized by electrospray mass spectrometry, EPR spectroscopy, and UV–visible spectroscopy, and the rates of catalytic oxygen-evolving activity were assayed. The use of  $\text{Mn}^{\text{II}}\text{LCl}_2$  precursors leads to higher product purity of the Mn dimers while achieving the 1:1 ligand to Mn stoichiometry appropriate for catalytic activity assay. These methods can be used to screen the catalytic activity of other di- $\mu$ -oxo dimanganese complexes generated by using a ligand library.

## Introduction

Bioinorganic model chemistry has played an important role in the understanding of the oxygen-evolving complex (OEC)<sup>1</sup> of photosystem II (PS II),<sup>2,3</sup> in which a tetrameric manganese cluster is known to catalyze the oxidation of water to molecular oxygen. Although it has been known for years that the manganese tetramer in PS II contains di- $\mu$ -oxo dimanganese units<sup>2,4</sup> and that water is the substrate of the

OEC, only a handful of di- $\mu$ -oxo manganese complexes have been synthesized that contain coordinated water.<sup>5–10</sup> Previously, we reported the  $\text{O}_2$ -evolving reactions catalyzed by  $[(\text{H}_2\text{O})\text{LMn}^{\text{III}}(\mu\text{-O})_2\text{Mn}^{\text{IV}}\text{L}(\text{OH}_2)]^{3+}$  ( $\text{L}$  = dipic, **1a**, and terpy, **1b**).<sup>7,11,12</sup> These complexes are functional models for the OEC with a biologically relevant  $\text{Mn}(\mu\text{-O})_2\text{Mn}$  core. The meridionally coordinating tridentate ligands allow water

\* To whom correspondence should be addressed. E-mail: gary.brudvig@yale.edu (G.W.B.); robert.crabtree@yale.edu (R.H.C.).

- (1) Abbreviations used in this report: EPR, electron paramagnetic resonance; ESI-MS, electrospray ionization mass spectrometry; OEC, oxygen-evolving complex; PS II, photosystem II; UV–vis, ultraviolet–visible spectroscopy; btp, 2,6-bis(benzimidazol-2'-yl)pyridine; bpy, 2,2'-bipyridine; Br-terpy, 4'-bromo-2,2':6',2''-terpyridine; Cl-terpy, 4'-chloro-2,2':6',2''-terpyridine; dipic, 2,6-dipicolinate; dpys, dipyrrodo-[4,3-b;5,6-b]acridine; EtO-terpy, 4'-ethoxy-2,2':6',2''-terpyridine; HO-terpy, 4'-hydroxy-2,2':6',2''-terpyridine;  $\text{Me}_2\text{N}$ -terpy, 4'-( $N,N$ -dimethylamino)-2,2':6',2''-terpyridine; mesityl-terpy, 4'-mesityl-2,2':6',2''-terpyridine; Ph-terpy, 4'-phenyl-2,2':6',2''-terpyridine; phen, 1,10-phenanthroline; py-phen, 2-(2'-pyridyl)-1,10-phenanthroline;  $t\text{Bu}_3$ -terpy, 4,4',4''-tri-*tert*-butyl-2,2':6',2''-terpyridine; terpy, 2,2':6',2''-terpyridine; tolyl-terpy, 4'-(4-methylphenyl)-2,2':6',2''-terpyridine.
- (2) Yachandra, V. K.; Sauer, K.; Klein, M. P. *Chem. Rev.* **1996**, 96, 2927.
- (3) Manchanda, R.; Brudvig, G. W.; Crabtree, R. H. *Coord. Chem. Rev.* **1995**, 144, 1.

- (4) Penner-Hahn, J. E. *Struct. Bonding* **1998**, 90, 1.
- (5) Chen, H. Y.; Faller, J. W.; Crabtree, R. H.; Brudvig, G. W. *J. Am. Chem. Soc.* **2004**, 126, 7345.
- (6) (a) Dave, B. C.; Czernuszewicz, R. S.; Bond, M. R.; Carrano, C. J. *Inorg. Chem.* **1993**, 32, 3593. (b) Reddy, K. R.; Rajasekharan, M. V.; Padhye, S.; Dahan, F.; Tuchagues, J. P. *Inorg. Chem.* **1994**, 33, 428.
- (7) Limburg, J.; Vrettos, J. S.; Liable-Sands, L. M.; Rheingold, A. L.; Crabtree, R. H.; Brudvig, G. W. *Science* **1999**, 283, 1524.
- (8) (a) Sarneski, J. E.; Thorp, H. H.; Brudvig, G. W.; Crabtree, R. H.; Schulte, G. K. *J. Am. Chem. Soc.* **1990**, 112, 7255. (b) Reddy, K. R.; Rajasekharan, M. V.; Arulsamy, N.; Hodgson, D. J. *Inorg. Chem.* **1996**, 35, 2283.
- (9) Suzuki, M.; Hayashi, Y.; Munezawa, K.; Suenaga, M.; Senda, H.; Uehara, A. *Chem. Lett.* **1991**, 1929.
- (10) Wiegardt, K.; Bossek, U.; Nuber, B.; Weiss, J.; Bonvoisin, J.; Corbella, M.; Vitols, S. E.; Girerd, J. J. *J. Am. Chem. Soc.* **1988**, 110, 7398.
- (11) Limburg, J.; Vrettos, J. S.; Chen, H. Y.; de Paula, J. C.; Crabtree, R. H.; Brudvig, G. W. *J. Am. Chem. Soc.* **2001**, 123, 423.
- (12) Limburg, J.; Brudvig, G. W.; Crabtree, R. H. *J. Am. Chem. Soc.* **1997**, 119, 2761.

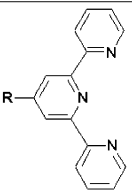
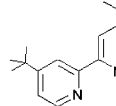
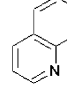
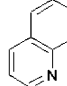
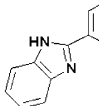
molecules to bind to the exchangeable sixth coordination site on each Mn; this leads to much more rapid O<sub>2</sub> evolution than seen for coordinatively saturated complexes such as [Mn<sup>III/IV</sup><sub>2</sub>(μ-O)<sub>2</sub>(bpy)<sub>4</sub>]<sup>3+</sup>.

To identify the steric and electronic factors that promote catalytic activity, it is important to expand the family of di-μ-oxo dimanganese complexes with terpy-like ligands and characterize their activity. So far, only two such complexes (L = dipic and terpy) have been characterized in solution and only the parent terpy Mn dimer complex has been successfully isolated. Attempts to expand this series using substituted terpy ligands were largely unsuccessful, mainly owing to the instability of the corresponding [Mn<sup>III/IV</sup><sub>2</sub>(μ-O)<sub>2</sub>(L)<sub>2</sub>(OH<sub>2</sub>)<sub>2</sub>]<sup>3+</sup> complexes in solution. In the cases where the Mn(III/IV) dimer complexes are stable (L = Ph-terpy and mesityl-terpy, reported in this study), the isolation process is tedious and often leads to low yields. Fast screening of a ligand library is, therefore, incompatible with this procedure.

An alternative way of testing catalytic activity is to prepare the Mn(III/IV) dimer complexes in situ, following the previous procedure that used a solution containing a mixture of ligand and MnCl<sub>2</sub> for the initial tests of **1a** and **1b**.<sup>12</sup> Because a wide range of organic species are known to be oxidized by high-valent oxo-Mn complexes<sup>13</sup> and because our recent results have shown that O<sub>2</sub> evolution is inhibited by the presence of excess free ligand during the catalysis,<sup>14</sup> Mn(III/IV) dimer solutions free of organic impurities and with a strict 1:1 ligand-to-Mn ratio are necessary for comparative analysis of the catalytic activity of a series of di-μ-oxo dimanganese complexes. Therefore, an easy and general synthesis of low-valent Mn complexes that can be used for the in situ preparation of Mn(III/IV) dimer solutions is needed.

An improved synthesis of Mn<sup>II</sup>LCl<sub>2</sub> was adapted from literature procedures for the synthesis of Mn(terpy)Cl<sub>2</sub>,<sup>15,16</sup> Mn(Ph-terpy)Cl<sub>2</sub>,<sup>17</sup> and related complexes.<sup>18–23</sup> It provides an easy way both to produce complexes in good yield without organic impurities and to achieve the desired ligand-to-Mn stoichiometry. Crystals of Mn<sup>II</sup>(Ph-terpy)Cl<sub>2</sub>, Mn<sup>II</sup>(mesityl-terpy)Cl<sub>2</sub>, and Mn<sup>II</sup>(dpva)Cl<sub>2</sub> were isolated and characterized

**Table 1.** Structures of Tridentate Ligands Used in This Study

Ligands	Abbreviations
	R = H terpy
	R = Cl Cl-terpy
	R = Br Br-terpy
	R = Ph Ph-terpy
	R = tolyl tolyl-terpy
	R = mesityl mesityl-terpy
	R = OEt EtO-terpy
	R = NMe <sub>2</sub> Me <sub>2</sub> N-terpy
	R = OH HO-terpy
	tBu <sub>3</sub> -terpy
	py-phen
	dpva
	bbp

by X-ray crystallography. The extensive Mn<sup>II</sup>LCl<sub>2</sub> family reported in this study could also be of interest for high-field EPR studies<sup>16</sup> and as bleaching catalysts for detergent applications.<sup>19–21</sup>

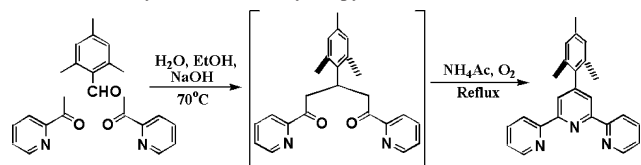
In addition, we report the in situ preparation of a series of di-μ-oxo dimanganese(III/IV) complexes [Mn<sup>III/IV</sup><sub>2</sub>(μ-O)<sub>2</sub>(L)<sub>2</sub>(X)<sub>2</sub>]<sup>3+</sup> (L = terpy, **1b**; Cl-terpy, **1c**; Br-terpy, **1d**; Ph-terpy, **1e**; tolyl-terpy, **1f**; mesityl-terpy, **1g**; tBu<sub>3</sub>-terpy, **1h**; EtO-terpy, **1i**; py-phen, **1j**; dpva, **1k**; Me<sub>2</sub>N-terpy, **1l**; HO-terpy, **1m**; and bbp, **1n** and X = a labile ligand such as water, chloride, or sulfate) from Mn<sup>II</sup>LCl<sub>2</sub> precursors (**2b–2n**, respectively). Table 1 shows the structures of the tridentate ligands. The resulting in situ solutions of **1** were characterized by EPR spectroscopy, UV–vis spectroscopy, and ESI-MS, and the catalytic activity of each of the in situ prepared solutions was determined. We obtained crystals of [Mn<sup>III/IV</sup><sub>2</sub>(μ-O)<sub>2</sub>(mesityl-terpy)<sub>2</sub>(OH<sub>2</sub>)<sub>2</sub>](NO<sub>3</sub>)<sub>3</sub>, and characterization of the structure by X-ray crystallography showed that the two Mn ions are crystallographically inequivalent. This dimer is very soluble in acetonitrile; having water molecules coordinated to the Mn ions, it allows studies in nonaqueous solutions where low-temperature experiments are possible and the concentration of water can be varied.

## Experimental Section

**Materials.** Me<sub>2</sub>N-terpy,<sup>24</sup> EtO-terpy,<sup>24</sup> Ph-terpy,<sup>17</sup> Br-terpy,<sup>25</sup> py-phen,<sup>26,27</sup> and dpva<sup>28</sup> were synthesized following literature procedures (Table 1). Oxone (2KHSO<sub>5</sub>·KHSO<sub>4</sub>·K<sub>2</sub>SO<sub>4</sub>) was purchased

- (13) Sarneski, J. E.; Michos, D.; Thorp, H. H.; Didiuk, M.; Poon, T.; Blewitt, J.; Brudvig, G. W.; Crabtree, R. H. *Tetrahedron Lett.* **1991**, 32, 1153.
- (14) Chen, H. Y. Ph.D. Thesis, Yale University, New Haven, 2004.
- (15) Harris, C. M.; Lockyer, T. N.; Stephens, N. C. *Aust. J. Chem.* **1966**, 19, 1741.
- (16) Mantel, C.; Baffert, C.; Romero, I.; Deronzier, A.; Pecaut, J.; Collomb, M. N.; Duboc, C. *Inorg. Chem.* **2004**, 43, 6455.
- (17) Constable, E. C.; Lewis, J.; Liptrot, M. C.; Raithby, P. R. *Inorg. Chim. Acta* **1990**, 178, 47.
- (18) Wang, S. X.; Zhu, Y.; Zhang, F. J.; Wang, Q. Y.; Wang, L. F. *Polyhedron* **1992**, 11, 1909.
- (19) Wieprecht, T.; Heinz, U.; Xia, J.; Schlingloff, G.; Dannacher, J. *J. Surfactants Deterg.* **2004**, 7, 59.
- (20) Wieprecht, T.; Xia, J. T.; Heinz, U.; Dannacher, J.; Schlingloff, G. *J. Mol. Catal. A-Chem.* **2003**, 203, 113.
- (21) Schlingloff, G.; Wieprecht, T.; Bachmann, F.; Dannacher, J.; Dubs, M. J.; Hazenkamp, M.; Richter, G.; Schmidt, B.; Schneider, A.; Weingartner, P. *PCT Int. Appl.* **2002**.
- (22) Hogg, R.; Wilkins, R. G. *J. Chem. Soc.* **1962**, 341.
- (23) Judge, J. S.; Reiff, W. M.; Intille, G. M.; Ballway, P.; Baker, W. A. *J. Inorg. Nucl. Chem.* **1967**, 29, 1711.

- (24) Constable, E. C.; Thompson, A.; Tocher, D. A.; Daniels, M. A. M. *New J. Chem.* **1992**, 16, 855.
- (25) Whittle, B.; Batten, S. R.; Jeffery, J. C.; Rees, L. H.; Ward, M. D. *J. Chem. Soc., Dalton Trans.* **1996**, 4249.
- (26) Hung, C. Y.; Wang, T. L.; Shi, Z. Q.; Thummel, R. P. *Tetrahedron* **1994**, 50, 10685.
- (27) Riesgo, E. C.; Jin, X. Q.; Thummel, R. P. *J. Org. Chem.* **1996**, 61, 3017.

**Scheme 1.** Synthesis of Mesityl-terpy.

from Acros Organics and was standardized using iodometric titrations. All other reagents were purchased from Aldrich and used without further purification. NMR spectra were recorded on Bruker DPX 400 and 500 MHz instruments. Elemental analyses were performed by Atlantic Microlabs, Inc., Norcross, GA.

**Synthesis of 4'-Mesityl-2,2':6',2''-terpyridine.** This ligand was prepared following the synthesis of Ph-terpy (Scheme 1).<sup>17</sup> 2-Acetylpyridine (18.9 mL, 0.17 mol) was added dropwise to a stirred mixture of mesitylaldehyde (10 g, 0.067 mol), EtOH (120 mL), and aqueous NaOH (1.5 M, 180 mL), was stirred at 70 °C for 3 days, was cooled to room temperature, and the mixture was extracted with  $\text{CHCl}_3$ . The extractant was washed with water three times and then evaporated to give a red oil. The red oil, presumably composed of 3-mesityl-1,5-bis(2-pyridyl)-1,5-pentanedione by comparison with the synthesis of Ph-terpy, was mixed with  $\text{NH}_4\text{Ac}$  (27 g, excess) and 300 mL of ethanol and then refluxed overnight with passage of air. The resulting blue solution was evaporated to a quarter of its original volume, water (100 mL) was added, and the mixture was extracted with  $\text{CHCl}_3$  ( $3 \times 100$  mL). Neutral alumina (30 g) was added to the combined  $\text{CHCl}_3$  extracts, and the resulting mixture was filtered through a packed neutral alumina layer. After the solid mixture was washed with copious diethyl ether, the combined filtrate was evaporated to give a crude mesityl-terpy product. Recrystallization from a 1:1  $\text{CH}_3\text{CN}/\text{CHCl}_3$  mixture gave colorless crystals (13.2 g, overall yield 56% based on mesitylaldehyde).  $^1\text{H}$  NMR (400 MHz,  $\text{CDCl}_3$ , 25 °C):  $\delta$  8.68 (m, 4H, Ar H), 8.31 (s, 2H, Ar H), 7.87 (t, 2H, Ar H), 7.33 (t, 2H, Ar H), 6.94 (s, 2H, Ar H), 2.34 (s, 3H,  $\text{CH}_3$ ), 2.08 (s, 6H,  $\text{CH}_3$ ).  $^{13}\text{C}$  NMR (400 MHz,  $\text{CDCl}_3$ , 25 °C):  $\delta$  156.3, 155.6, 151.8, 149.2, 137.1, 136.8, 136.7, 135.1, 128.2, 123.8, 122.1, 121.3, 21.11, 20.77. Anal. Calcd for  $\text{C}_{24}\text{H}_{21}\text{N}_3$ : C, 82.02; H, 6.02; N, 11.96. Found: C, 81.80; H, 5.99; N, 11.96.

**Preparation of  $\text{Mn}^{\text{II}}\text{LCl}_2$  Complexes. Method A.** The ligand L (0.43 mmol) was completely dissolved in a minimum amount of hot acetone (typically 20 mL, 50 °C), and a solution of  $\text{MnCl}_2 \cdot 4\text{H}_2\text{O}$  (2.2 mmol) in methanol (5 mL) was then added. A yellow precipitate formed immediately, except for  $\text{L} = t\text{Bu}_3\text{-terpy}$ , where the precipitate formed after several minutes. The resulting suspension was allowed to ripen for 0.5–24 h at 50 °C and cooled to 0 °C. The precipitate was filtered and washed first with a 1:4 v/v methanol–acetone mixture ( $3 \times 0.5$  mL) and then with copious diethyl ether. Drying the precipitate under vacuum overnight gave  $\text{Mn}^{\text{II}}\text{LCl}_2$  with good purity and yields. Typical yields are 70–98% (Table 2). Yellow crystals of  $\text{Mn}(\text{Ph-terpy})\text{Cl}_2$  suitable for X-ray analysis were obtained by slow evaporation of a solution of  $\text{Mn}(\text{Ph-terpy})\text{Cl}_2$  in a 1:1 acetonitrile–methanol mixture. Orange crystals of  $\text{Mn}(\text{dpys})\text{Cl}_2$  suitable for X-ray analysis were obtained by slow evaporation of a mixed solution of  $\text{MnCl}_2$  (2 mM) and dpys (2 mM) in a 1:1 acetonitrile–water mixture.

**Method B.** Mesityl-terpy (0.676 g, 1.9 mmol) was suspended in 5 mL of heated  $\text{CH}_3\text{CN}$ , to which a concentrated aqueous  $\text{MnCl}_2 \cdot 4\text{H}_2\text{O}$  (3 M, 5 mL, large excess) solution was added. Owing to the high density and ionic strength of the  $\text{MnCl}_2$  solution, the aqueous

solution forms a colorless layer beneath the deep yellow acetonitrile layer. Within minutes, crystals of **2g** precipitate out and float between the two layers. This mixture was refluxed for 3 h with vigorous stirring and then cooled to room temperature. The resulting yellow crystalline precipitate was filtered and washed with cold, dilute aq  $\text{MnCl}_2$  (0.1 M,  $3 \times 1$  mL), cold acetonitrile ( $3 \times 1$  mL), and then with copious diethyl ether. Drying under vacuum overnight gave  $\text{Mn}^{\text{II}}(\text{mesityl-terpy})\text{Cl}_2$  with good purity (0.729 g, 79%, Table 2). Crystals of  $\text{Mn}(\text{mesityl-terpy})\text{Cl}_2$  were selected directly from this product for X-ray crystallographic analysis.

The  $\text{Mn}(\text{bbp})\text{Cl}_2$  complex (**2n**) was prepared as previously described.<sup>18</sup>

**General Procedure for the in situ Preparation of  $[\text{Mn}^{\text{III/IV}}_2(\mu\text{-O})_2(\text{L})_2(\text{X})_2]^{3+}$  (**1b–1n**).** A 0.75–2 mM solution of  $\text{Mn}^{\text{II}}\text{LCl}_2$  in a 1:1 acetonitrile–water mixture was cooled to 0 °C. To this solution was added an equal volume of 0.56–1.5 mM (0.75 equiv) oxone in water. The solution turned deep green within 10 min.

**Preparation of  $[\text{Mn}^{\text{III/IV}}_2(\mu\text{-O})_2(\text{L})_2(\text{H}_2\text{O})_2](\text{NO}_3)_3$  (**L** = Ph-terpy (**1e**) and mesityl-terpy (**1g**)).** A mixture of L (0.282 mmol, 1.05 equiv),  $\text{MnCl}_2 \cdot 4\text{H}_2\text{O}$  (0.269 mmol, 20 mL, 1 equiv), and  $\text{KNO}_3$  (5 g) in a mixture of  $\text{CH}_3\text{CN}$  and  $\text{H}_2\text{O}$  (25 and 20 mL, respectively) was stirred at 50 °C until all reactants were dissolved to form a yellow solution. After the solution was cooled in an ice bath, oxone (0.202 mmol, 0.75 equiv) dissolved in 5 mL of  $\text{H}_2\text{O}$  was added with stirring. The solution turned deep green in a few minutes and was allowed to stir for an extra 5 min in the ice bath. The majority of the  $\text{CH}_3\text{CN}$  in solution was then removed in vacuo, as estimated by the decrease of the total volume, and the resulting green precipitate was quickly filtered off and washed first with a cold 1:5 acetonitrile–water mixture ( $3 \times 0.5$  mL) and then with copious diethyl ether. Drying under vacuum overnight gave the desired product.

**1e.** 105 mg of Ph-terpy and 64 mg of  $\text{MnCl}_2 \cdot 4\text{H}_2\text{O}$  gave 52 mg of **1e** (33% yield according to  $\text{MnCl}_2 \cdot 4\text{H}_2\text{O}$ ). Anal. Calcd for  $\text{C}_{42}\text{H}_{34}\text{Mn}_2\text{N}_9\text{O}_{13}$ : C, 51.34; H, 3.49; N, 12.83. Found: C, 51.63; H, 3.58; N, 12.82.

**1g.** 99 mg of mesityl-terpy and 53 mg of  $\text{MnCl}_2 \cdot 4\text{H}_2\text{O}$  gave 75 mg of **1g** (52% yield according to  $\text{MnCl}_2 \cdot 4\text{H}_2\text{O}$ ). Anal. Calcd for  $\text{C}_{48}\text{H}_{46}\text{Mn}_2\text{N}_9\text{O}_{13}$ : C, 54.04; H, 4.35; N, 11.82. Found: C, 54.32; H, 4.33; N, 11.62.

Following similar procedures, but with 1.20 equiv of mesityl-terpy, a 1 mM solution of **1g** was prepared in 1:1 acetonitrile–water mixture. Slow evaporation of this solution gave black-green crystals of **1g** suitable for X-ray analysis.

**Crystal Structure Determination of  $\text{Mn}(\text{Ph-terpy})\text{Cl}_2$  (**2e**),  $\text{Mn}(\text{mesityl-terpy})\text{Cl}_2$  (**2g**),  $\text{Mn}(\text{dpys})\text{Cl}_2$  (**2k**), and  $[\text{Mn}_2(\mu\text{-O})_2(\text{mesityl-terpy})_2(\text{OH}_2)_2](\text{NO}_3)_3$  (**1g**).** All diffraction data were collected on a Nonius KappaCCD diffractometer with graphite monochromated Mo  $\text{K}\alpha$  radiation. ORTEP diagrams are shown in Figures 1–3, and the crystallographic data are presented in Table 3. Crystals of complexes with approximate dimensions  $0.20 \times 0.10 \times 0.08$  mm<sup>3</sup> for **2e**,  $0.15 \times 0.10 \times 0.10$  mm<sup>3</sup> for **2g**,  $0.3 \times 0.3 \times 0.3$  mm<sup>3</sup> for **2k**, and  $0.07 \times 0.19 \times 0.20$  mm<sup>3</sup> for **1g** were mounted with epoxy cement on the tips of fine glass fibers. All data were corrected for Lorentz and polarization effects. The structures were solved by direct methods and expanded using Fourier techniques.<sup>29</sup> The non-hydrogen atoms were refined anisotropically. Hydrogen atoms were included in calculated positions except for **2k** for which hydrogen atoms were refined isotropically.

**Electrospray Ionization Mass Spectrometry.** ESI-MS spectra were collected on a Waters/Micromass ZQ 4000 mass spectrometer.

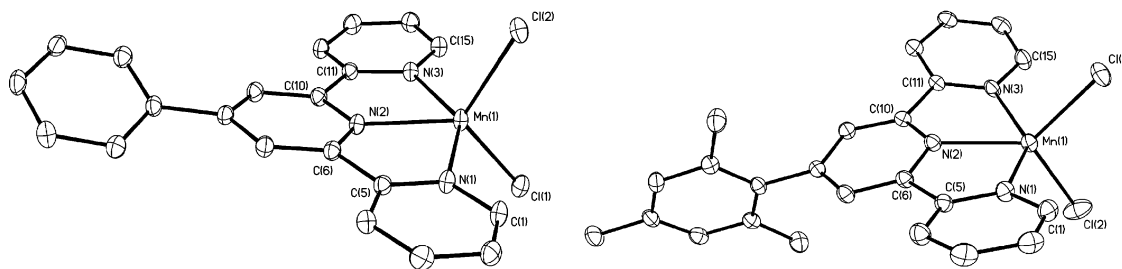
(28) Hung, C. Y.; Wang, T. L.; Jang, Y. C.; Kim, W. Y.; Schmehl, R. H.; Thummel, R. P. *Inorg. Chem.* **1996**, *35*, 5953.

(29) Vandersluijs, P.; Spek, A. L. *Acta Crystallogr. A* **1990**, *46*, 194.



**Table 2.** Preparation of  $\text{Mn}^{\text{II}}\text{LCI}_2$  Complexes

entry	no.	formula	method	yield	elemental analysis	
$\text{Mn}(\text{terpy})\text{Cl}_2$	<b>2b</b>	$\text{C}_{15}\text{H}_{11}\text{Cl}_2\text{MnN}_3$	A	96%	calcd	C, 50.17; H, 3.09; N, 11.70
					found	C, 50.03; H, 3.10; N, 11.70
$\text{Mn}(\text{Cl-terpy})\text{Cl}_2$	<b>2c</b>	$\text{C}_{15}\text{H}_{10}\text{Cl}_3\text{MnN}_3$	A	96%	calcd	C, 45.78; H, 2.56; N, 10.68
					found	C, 45.81; H, 2.53; N, 10.44
$\text{Mn}(\text{Br-terpy})\text{Cl}_2$	<b>2d</b>	$\text{C}_{15}\text{H}_{10}\text{BrCl}_2\text{MnN}_3$	A	80%	calcd	C, 41.13; H, 2.30; N, 9.59
					found	C, 40.86; H, 2.28; N, 9.58
$\text{Mn}(\text{Ph-terpy})\text{Cl}_2$	<b>2e</b>	$\text{C}_{21}\text{H}_{15}\text{Cl}_2\text{MnN}_3$	A	96%	calcd	C, 57.96; H, 3.47; N, 9.66
					found	C, 57.95; H, 3.40; N, 9.65
$\text{Mn}(\text{tolyl-terpy})\text{Cl}_2$	<b>2f</b>	$\text{C}_{22}\text{H}_{17}\text{Cl}_2\text{MnN}_3$	A	98%	calcd	C, 58.82; H, 3.81; N, 9.35
					found	C, 58.40; H, 3.88; N, 9.31
$\text{Mn}(\text{mesityl-terpy})\text{Cl}_2$	<b>2g</b>	$\text{C}_{24}\text{H}_{21}\text{Cl}_2\text{MnN}_3$	B	79%	calcd	C, 60.39; H, 4.43; N, 8.80
					found	C, 60.28; H, 4.48; N, 8.94
$\text{Mn}(t\text{Bu}_3\text{-terpy})\text{Cl}_2$	<b>2h</b>	$\text{C}_{27}\text{H}_{35}\text{Cl}_2\text{MnN}_3$	A	73%	calcd	C, 61.48; H, 6.69; N, 7.97
					found	C, 61.56; H, 6.76; N, 7.86
$\text{Mn}(\text{EtO-terpy})\text{Cl}_2$	<b>2i</b>	$\text{C}_{17}\text{H}_{15}\text{Cl}_2\text{MnN}_3\text{O}$	A	77%	calcd	C, 50.64; H, 3.75; N, 10.42
					found	C, 50.54; H, 3.72; N, 10.46
$\text{Mn}(\text{py-phen})\text{Cl}_2$	<b>2j</b>	$\text{C}_{17}\text{H}_{11}\text{Cl}_2\text{MnN}_3$	A	87%	calcd	C, 53.29; H, 2.89; N, 10.97
					found	C, 53.52; H, 2.92; N, 11.04
$\text{Mn}(\text{dpya})\text{Cl}_2$	<b>2k</b>	$\text{C}_{19}\text{H}_{11}\text{Cl}_2\text{MnN}_3$	A	85%	calcd	C, 56.05; H, 2.72; N, 10.32
					found	C, 56.05; H, 2.65; N, 10.34
$\text{Mn}(\text{Me}_2\text{N-terpy})\text{Cl}_2$	<b>2l</b>	$\text{C}_{17}\text{H}_{16}\text{Cl}_2\text{MnN}_4$	A	70%	calcd	C, 50.77; H, 4.01; N, 13.93
					found	C, 50.67; H, 3.97; N, 14.01
$\text{Mn}(\text{HO-terpy})\text{Cl}_2$	<b>2m</b>	$\text{C}_{15}\text{H}_{11}\text{Cl}_2\text{MnN}_3\text{O}$	A	90%	calcd	C, 48.03; H, 2.96; N, 11.20
					found	C, 48.11; H, 3.01; N, 11.27

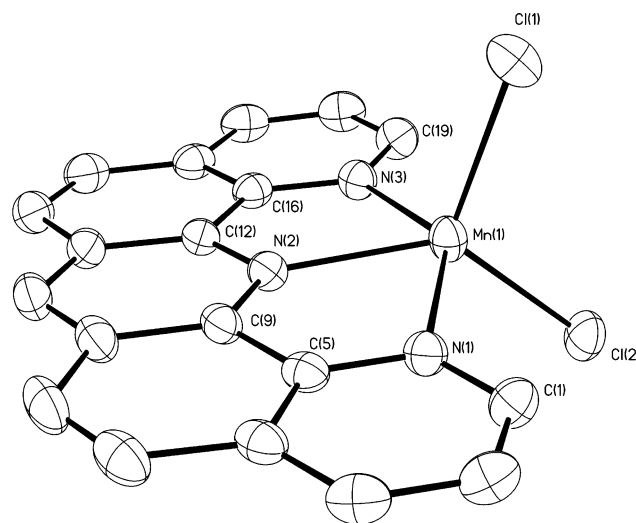
**Figure 1.** ORTEP diagrams of  $\text{Mn}^{\text{II}}(\text{Ph-terpy})\text{Cl}_2$  (**2e**) and  $\text{Mn}^{\text{II}}(\text{mesityl-terpy})\text{Cl}_2$  (**2g**), showing 30% probability thermal ellipsoids. Hydrogen atoms are omitted for clarity.

Owing to the weak signal at high mass, multiple scans over a narrow mass range were required to obtain a good signal/noise ratio. To obtain simulated spectra, a Gaussian peak was fitted to the highest observed peak by varying mass ( $M$ ), peak width, and peak area. A group of Gaussian peaks was then generated at mass =  $M \pm n$  ( $n$  = integers) with the same peak width and with peak areas adjusted to the calculated isotope ratios. Isotope ratios were calculated using Masslynx (V4.0) and the isotope distribution calculator at <http://www.sisweb.com/mstools.htm>.

**UV–Vis Spectroscopy.** UV–vis spectra were recorded on a Varian Cary-3E UV–visible spectrophotometer at room temperature using a 1 cm path length cuvette.

**EPR Spectroscopy.** Perpendicular-mode EPR spectra were collected on an X-band Bruker E-500 spectrometer equipped with a SHQ cavity and an Oxford ESR-900 liquid helium cryostat. In situ solutions of **1** were diluted with an equivalent volume of NaOAc/HOAc buffer, pH = 4.5; aliquots (250  $\mu\text{L}$ ) of this mixture were transferred to EPR tubes, and were frozen in liquid nitrogen. All in situ solutions were frozen within 10 min of mixing for the EPR measurements. Spectra used for quantitation were collected at 10 K with the following settings: microwave frequency, 9.38 GHz; microwave power, 1 mW; field modulation amplitude, 2 G; field modulation frequency, 100 kHz; and time constant, 0.3 s. Spectra shown in Figure 6 were collected with a field modulation amplitude of 20 G.

The quantitation of the yields of the  $[\text{Mn}^{\text{III/IV}}_2(\text{O})_2\text{L}_2\text{X}_2]^{3+}$  complexes obtained in situ from  $\text{Mn}^{\text{II}}\text{LCI}_2$  precursors was done by measuring the peak-to-trough height of the lowest field hyperfine

**Figure 2.** ORTEP diagram of  $\text{Mn}^{\text{II}}(\text{dpya})\text{Cl}_2$  (**2k**), showing 30% probability thermal ellipsoids. Hydrogen atoms are omitted for clarity. Selected bond distances ( $\text{\AA}$ ) and bond angles (deg):

$\text{Mn}(1)-\text{N}(1)$	2.32	$\text{Mn}(1)-\text{N}(2)$	2.19
$\text{N}(1)-\text{C}(5)$	1.36	$\text{C}(5)-\text{C}(9)$	1.44
$\text{C}(12)-\text{C}(16)$	1.44	$\text{C}(16)-\text{N}(3)$	1.36
$\text{Mn}(1)-\text{N}(3)$	2.34	$\text{Mn}(1)-\text{Cl}(2)$	2.33
$\text{C}(9)-\text{N}(2)$	1.34	$\text{N}(2)-\text{C}(12)$	1.34
$\text{N}(1)-\text{C}(5)-\text{C}(9)$	117	$\text{C}(5)-\text{C}(9)-\text{N}(2)$	116.1
$\text{N}(1)-\text{C}(12)-\text{C}(16)$	116.6	$\text{C}(12)-\text{C}(16)-\text{N}(3)$	116.6

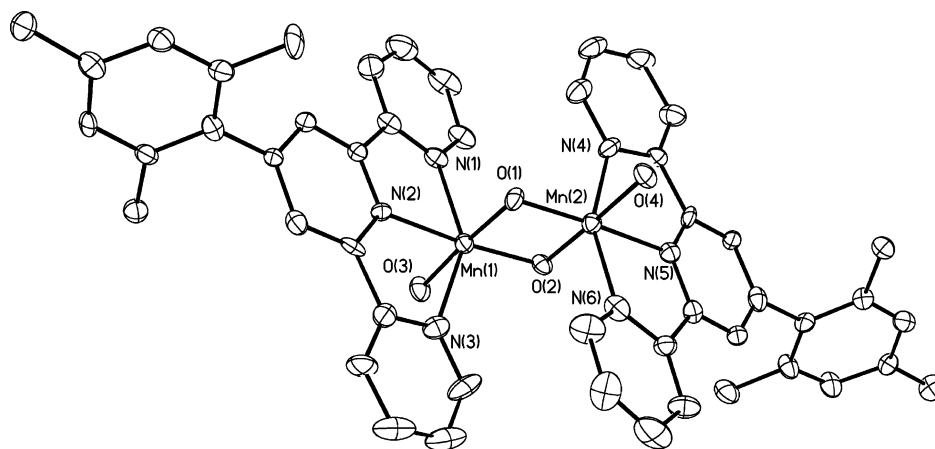


**Figure 3.** ORTEP diagram of  $[\text{Mn}_2(\mu\text{-O})_2(\text{mesityl-terpy})_2(\text{OH})_2](\text{NO}_3)_3$  (**1g**), showing 30% probability thermal ellipsoids. Hydrogen atoms, nitrate counterions, and waters of crystallization are omitted for clarity. Selected bond distances (Å):

Mn(1)–N(1) <sub>ax</sub>	2.22	Mn(1)–N(2) <sub>eq</sub>	2.05
Mn(1)–N(3) <sub>ax</sub>	2.19	Mn(1)–O(1) <sub>eq</sub>	1.84
Mn(1)–O(2) <sub>eq</sub>	1.81	Mn(1)–O(3) <sub>eq</sub>	2.00
Mn(2)–N(4) <sub>ax</sub>	2.04	Mn(2)–N(5) <sub>eq</sub>	2.04
Mn(2)–N(6) <sub>ax</sub>	2.06	Mn(2)–O(1) <sub>eq</sub>	1.81
Mn(2)–O(2) <sub>eq</sub>	1.76	Mn(2)–O(4) <sub>eq</sub>	1.99
Mn(1)⋯Mn(2)	2.72		

**Table 3.** X-Ray Crystallographic Data for **1g**·6H<sub>2</sub>O, **2e**, **2g**, and **2k**

	<b>1g</b> ·6H <sub>2</sub> O	<b>2e</b>	<b>2g</b>	<b>2k</b>
empirical formula	C <sub>48</sub> H <sub>58</sub> Mn <sub>2</sub> N <sub>9</sub> O <sub>19</sub>	C <sub>21</sub> H <sub>15</sub> Cl <sub>2</sub> MnN <sub>3</sub>	C <sub>24</sub> H <sub>21</sub> Cl <sub>2</sub> MnN <sub>3</sub>	C <sub>19</sub> H <sub>11</sub> Cl <sub>2</sub> MnN <sub>3</sub>
fw	1174.91	435.20	477.28	407.16
cryst syst	triclinic	monoclinic	monoclinic	triclinic
space group	<i>P</i> 1̄(# 2)	<i>P</i> 2 <sub>1</sub> (1)/ <i>n</i> (# 14)	<i>P</i> 2 <sub>1</sub> (1)/ <i>c</i> (# 14)	<i>P</i> 1̄(# 2)
<i>a</i> , Å	7.9563(3)	12.160(2)	11.694(2)	7.5455(15)
<i>b</i> , Å	13.3147(4)	9.756(2)	12.843(3)	9.5624(19)
<i>c</i> , Å	25.5000(7)	16.676(3)	14.854(3)	12.599(3)
$\alpha$ , deg	80.666(2)	90	90	95.91(3)
$\beta$ , deg	86.254(2)	106.68(3)	97.59(3)	97.55(3)
$\gamma$ , deg	84.000(2)	90	90	110.33(3)
<i>V</i> , Å <sup>3</sup>	2647.8(1)	1895.0(7)	2211.2(8)	834.2(3)
<i>Z</i>	2	4	4	2
<i>T</i> , °C	−90(1)	−100(2)	−100(2)	23(2)
$\lambda$ , Å	0.71069	0.71073	0.71073	0.71073
<i>d</i> <sub>cal</sub> , g/cm <sup>3</sup>	1.461	1.525	1.434	1.621
<i>F</i> <sub>000</sub>	1202.00	884	980	410
no. of rflns				
total/unique	30 050/12 043	7869/4662	10 103/5448	5404/3930
no. observations				
( <i>I</i> > 3.00σ( <i>I</i> ))	4921	4662	5448	3930
refln/param ratio	7.00	19.11	19.39	17.39
<i>R</i> ; <i>R</i> <sub>w</sub>	0.068 <sup>a</sup> ; 0.087 <sup>b</sup>	0.041 <sup>a</sup> ; 0.081 <sup>c</sup>	0.046 <sup>a</sup> ; 0.106 <sup>c</sup>	0.040 <sup>a</sup> ; 0.078 <sup>c</sup>
GO <sup>c</sup>				
indicator	2.17	1.006	1.017	1.003

$$^a R = \sum ||F_o| - |F_c|| / \sum |F_o|; \quad ^b R_w = [\sum w(|F_o| - |F_c|)^2 / \sum w F_o^2]^{1/2}; \quad ^c R_w = \{\sum [w(F_o^2 - F_c^2)^2] / \sum w(F_o^2)^2\}^{1/2}.$$

line in the 16-line EPR signal characteristic of di- $\mu$ -oxo Mn(III/IV) compounds. This hyperfine line was chosen to minimize interference from Mn(II) species in solution. The yield of each di- $\mu$ -oxo Mn(III/IV) complex was determined by reference to the peak to trough height of the 16-line EPR signal obtained for a solution of **1g** prepared from the pure complex with the same total manganese concentration as in the *in situ* experiments. A solution of **1g** with tetrabutylammonium chloride added to a final concentration of two chlorides per manganese was also tested in the same way to check for the effect of chloride ions on the EPR signal of the  $[\text{Mn}^{\text{III/IV}}_2(\text{O})_2\text{L}_2\text{X}_2]^{3+}$  complex. The results for **1g** with and without added tetrabutylammonium chloride were identical within experimental error.

**Oxygen Evolution Assays.** The rates of oxygen evolution from solutions of the  $[\text{Mn}^{\text{III/IV}}_2(\text{O})_2\text{L}_2\text{X}_2]^{3+}$  complexes were measured at 298 K by a YSI standard oxygen probe (Clark Electrode) attached to a Cole–Parmer chart recorder using oxone as the oxidant as previously described.<sup>11</sup> The *in situ* experiments were done by mixing a 7.2 mM solution of the Mn(II)LCl<sub>2</sub> complex in a 1:1 (v/v) acetonitrile–water mixture with an equal volume of a 5.4 mM (0.75 equiv) aqueous solution of oxone at 0 °C. After waiting a few minutes for formation of the  $[\text{Mn}^{\text{III/IV}}_2(\text{O})_2\text{L}_2\text{X}_2]^{3+}$  complex, as evidenced by the solution turning green, a 50  $\mu\text{L}$  aliquot was injected into 6 mL of an aqueous solution of 15 mM oxone stirring beneath the Clark electrode. Thus, solutions of manganese complexes were in a 1:3 acetonitrile–water mixture before injection

into the Clark electrode cell, except in the case of **2e**, which was in a 3:1 acetonitrile–water mixture. This was done in order to compare with the solution of the authentic dimer **1e**, which was not soluble in 1:3 acetonitrile–water but was soluble in 3:1 acetonitrile–water (see below). A 25% excess of mesityl-terpy ligand and oxone (above what is calculated for stoichiometric conversion of Mn(II) to Mn<sub>2</sub>(III/IV)) was used with **2g**, as mesityl-terpy was observed to undergo relatively fast oxidation in the presence of oxone (data not shown). The pure complex **1b** was dissolved in a 1:3 acetonitrile–water mixture to a concentration of 3.6 mM total manganese. Fifty microliters of this solution was injected into 6 mL of a 15 mM aqueous solution of oxone stirring beneath the Clark electrode. The reported rates are normalized to the rate obtained for this sample. A solution of pure **1e** (3.6 mM manganese in 3:1 acetonitrile–water) was also assayed for comparison to the di- $\mu$ -oxo dimanganese complex generated in situ from a solution of **2e**. Finally, a solution of pure **1g** (3.6 mM manganese in 1:3 acetonitrile–water) was prepared with 25% excess ligand per manganese and excess oxone (as above, for **2g**) and assayed for comparison to the di- $\mu$ -oxo dimanganese complex generated in situ from a solution of **2g**.

## Results and Discussion

**Synthesis of Mesityl-terpy.** The synthesis of mesityl-terpy via Suzuki coupling of Br-terpy with a suitable boron reagent was reported in the recent literature.<sup>30,31</sup> By following the procedure for synthesis of Ph-terpy,<sup>17</sup> we were able to synthesize mesityl-terpy by this better route (Scheme 1). The reaction conditions were only slightly modified, although the separation methods for products are different, owing to the difference in solubility. Heating during the first step was necessary to improve the overall yield (22% to 56%), possibly by overcoming the sterically demanding second Michael addition of 2-acetylpyridine to mesitylaldehyde.<sup>31</sup> Using this method, a large-scale synthesis from commercially available starting materials is achieved.

**Synthesis and Characterization of Mn<sup>II</sup>LCl<sub>2</sub> (**2**).** The two preparative methods used for the syntheses of Mn<sup>II</sup>LCl<sub>2</sub> were adapted from previous work.<sup>15,17,18</sup> Method A generally provided pure product in high yield, as the ligand was fully dissolved in acetone and MnCl<sub>2</sub> in methanol while the product Mn<sup>II</sup>LCl<sub>2</sub> has a low solubility in the final 4:1 acetone–methanol mixture. However, Mn<sup>II</sup>(mesityl-terpy)-Cl<sub>2</sub> is very soluble in the 4:1 acetone–methanol mixture, so method B was, therefore, used for its synthesis. This method uses a minimum amount of acetonitrile–water mixture, in which the mesityl-terpy was not completely dissolved. Long reflux is necessary to ensure complete reaction. In both methods, a large excess of MnCl<sub>2</sub> was used to suppress [Mn<sup>II</sup>(L)<sub>2</sub>]<sup>2+</sup> formation and to decrease the solubility of Mn<sup>II</sup>LCl<sub>2</sub>. The Mn<sup>II</sup>LCl<sub>2</sub> complexes usually precipitate as fine particles, and incubation at elevated temperature is needed to render them suitable for filtration. In some cases, for example with *t*Bu<sub>3</sub>-terpy, a significant amount of the fine precipitate was lost during filtration, even after ripening; this leads to lower

yields. Following either method A or B, a small amount of organic impurity and the excess MnCl<sub>2</sub> are expected to remain dissolved in the solvent mixture and to be removed on isolation.

In contrast to the stability of Mn<sup>II</sup>(terpy)Cl<sub>2</sub> in aqueous solution, the dissolution of many of the new Mn<sup>II</sup>LCl<sub>2</sub> complexes (L = Cl-terpy, Br-terpy, ph-terpy, tolyl-terpy, mesityl-terpy, *t*Bu<sub>3</sub>-terpy, and bbp) in water leads to precipitation of the ligands within minutes. This is surprising since it is generally believed that the ligation of tridentate terpy-type ligands to Mn<sup>2+</sup> is strong and that the substituent groups at positions far from the metal binding site would cause only minor changes in the chemical and physical properties of the Mn<sup>II</sup>LCl<sub>2</sub> complexes. De-coordination may be driven by precipitation of the ligand, however. Although acetonitrile is generally not a good solvent for either the ligands or the MnLCl<sub>2</sub> complexes, all the Mn<sup>II</sup>LCl<sub>2</sub> complexes are soluble and stable in a 1:1 mixture of acetonitrile and water. Mn(II) complexes with less-hydrophobic ligands (EtO-terpy, Me<sub>2</sub>N-terpy, HO-terpy, py-phen, and dpva) are similar to Mn(terpy)Cl<sub>2</sub> in solubility and stability in aqueous solution.

Figures 1 and 2 show the crystal structures of Mn(Ph-terpy)Cl<sub>2</sub> (**2e**), Mn(mesityl-terpy)Cl<sub>2</sub> (**2g**), and Mn(dpva)-Cl<sub>2</sub> (**2k**). The major difference between the structures of **2e** and **2g** is that the more sterically demanding mesityl group of **2g** tilts at a larger angle to the terpy plane (dihedral angles between the central pyridine ring and its aromatic pendant are 21.9° and 74.8° for **2e** and **2g**, respectively). This effect appears to prevent close stacking of **2g** in the crystal structure; the inefficient stacking contributes to the smaller calculated density of **2g** (1.434 g/cm<sup>3</sup>) versus **2b**, **2e**, and **2k** (1.614, 1.525, and 1.621 g/cm<sup>3</sup>, respectively), and may contribute to the higher solubility of **2g** in organic solvents. Compared to the trigonal bipyramidal geometry of Mn<sup>II</sup>-(terpy)X<sub>2</sub> (X = Br (**3**) and I (**4**))<sup>16</sup> and the distorted square pyramidal geometry of **2b**<sup>16</sup> and **2n**,<sup>18</sup> the geometries of Mn<sup>II</sup> in **2e**, **2g**, and **2k** are between the two geometries. This is evident from Table 4; the X(1)–Mn(1)–N(2) and X(2)–Mn(1)–N(2) angles of **2e**, **2g**, and **2k** are between the corresponding angles of **2b** and the equivalent angles of **3** and **4**. Interestingly, Cl(1) of **2g** is disordered over two positions with an occupancy factor ratio of 60:40. With Cl(1) at one position, the Cl(1)–Mn(1)–N(2) and Cl(2)–Mn(1)–N(2) angles are almost equivalent, while at the other position they are not. The absence of ligand-field effects for a d<sup>5</sup> high-spin Mn(II) clearly allows packing forces to distort those structures.

The ligand dpva differs from terpy only by two etheno bridges (Table 1) which fuse the three pyridine rings and appear to prevent the outer pyridine rings from tilting toward the central pyridine ring. For example, the N(1)–C(5)–C(9), C(5)–C(9)–N(2), N(2)–C(12)–C(16), and C(12)–C(16)–N(3) angles of **2k** (117.0°, 116.1°, 116.6°, and 116.6°, respectively) are larger than the corresponding angles in Mn<sup>II</sup>-(terpy)Cl<sub>2</sub> (**2b**, 115.4°, 114.9°, 114.4°, and 115.5°, respectively). This leads to an increase of the N(1)–N(3) distances from **2b** (4.28 Å) to **2k** (4.42 Å) even though the C–C bond

(30) Goodall, W.; Wild, K.; Arm, K. J.; Williams, J. A. G. *J. Chem. Soc., Perkin Trans. 2* **2002**, 1669.

(31) Leslie, W.; Batsanov, A. S.; Howard, J. A. K.; Williams, J. A. G. *Dalton Trans.* **2004**, 623.

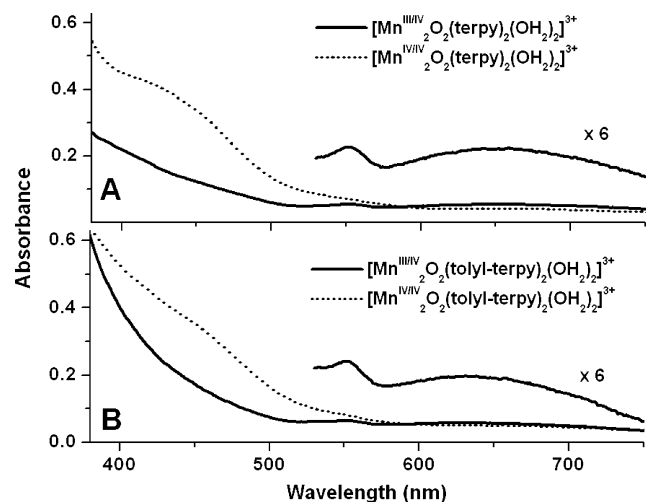


**Figure 4.** Selected UV-vis spectra (0 °C) of Mn(III/IV) and Mn(IV/IV) dimers prepared in situ with meridionally coordinating ligand terpy (A) and tolyl-terpy (B). Similar absorption bands were also observed for L = Cl-terpy, Br-terpy, Ph-terpy, mesityl-terpy, *t*Bu<sub>3</sub>-terpy, and EtO-terpy.

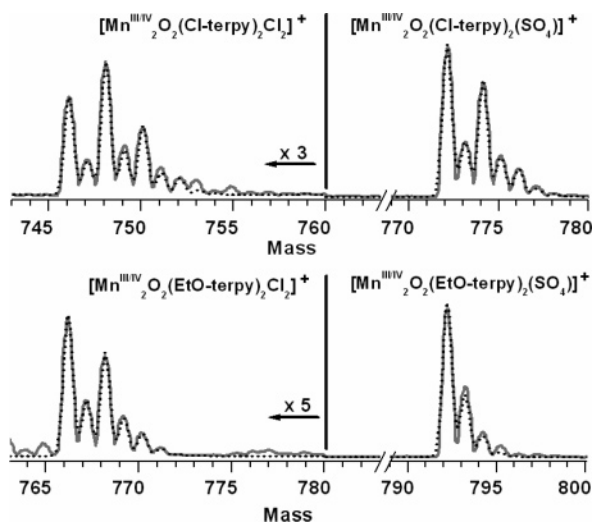


**Figure 5.** Selected ESI-MS data showing  $[\text{Mn}^{\text{III/IV}}_2(\mu\text{-O})_2(\text{L})_2\text{Cl}_2]^+$  and  $[\text{Mn}^{\text{III/IV}}_2(\mu\text{-O})_2(\text{L})_2(\text{SO}_4)]^+$  for L = Cl-terpy and EtO-terpy. Dotted lines show the simulated spectra in both cases. Corresponding peaks were also observed for L = terpy, Br-terpy, Ph-terpy, tolyl-terpy, mesityl-terpy, *t*Bu<sub>3</sub>-terpy, and py-phen.

distance between the adjacent pyridine rings decreases from 1.49 to 1.44 Å.

**In Situ Preparation of  $[\text{Mn}^{\text{III/IV}}_2(\text{O})_2\text{L}_2\text{X}_2]^{3+}$ .** One major difficulty in the synthesis of **1** was ligation of all free  $\text{Mn}^{2+}$  before the addition of an oxidant, otherwise the oxidation of uncoordinated  $\text{Mn}^{2+}$  always led to rapid and irreversible precipitation of  $\text{MnO}_2$ . These initial attempts failed because in aqueous solution most of the terpy derivatives do not form stable complexes with  $\text{Mn}^{2+}$  (vide supra). A 1:1 acetonitrile–water solvent mixture provides good solubility and stability for  $\text{Mn}^{\text{II}}\text{LCl}_2$  complexes and is resistant to oxidation by high-valent Mn complexes. To minimize  $\text{O}_2$  evolution catalyzed by the initially formed **1** when oxone was added to oxidize the Mn(II) complexes to the Mn(III,IV) dimers, the  $\text{MnLCl}_2$  solutions were cooled to 0 °C to slow  $\text{O}_2$  evolution and allow complete mixing with the oxone solution.

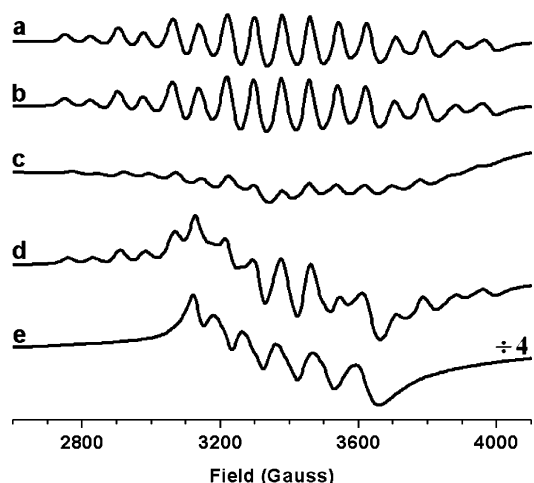


**Figure 6.** Selected EPR spectra showing the preparation of  $[\text{Mn}^{\text{III/IV}}_2(\mu\text{-O})_2(\text{L})_2(\text{X})_2]^{3+}$  in situ from  $\text{Mn}^{\text{II}}\text{LCl}_2$  and oxone, with L = (a) terpy, (b) Cl-terpy, (c) dpya, (d) Me<sub>2</sub>N-terpy, and (e) HO-terpy. Mixed-valence Mn(III/IV) dimers were also prepared for L = EtO-terpy, Br-terpy, Ph-terpy, tolyl-terpy, mesityl-terpy, and *t*Bu<sub>3</sub>-terpy; their corresponding 16-line spectra were analogous to those in (a) and (b) and, therefore, are not shown here. When L = py-phen, the EPR spectrum of the corresponding in situ solution of **1j** was similar to that in (c), but with a slightly stronger 16-line signal. The in situ yields of  $[\text{Mn}^{\text{III/IV}}_2(\mu\text{-O})_2(\text{L})_2(\text{X})_2]^{3+}$  for all of the ligands are listed in Table 5.

Shortly after the addition 0.75 equiv of oxone solution,  $\text{MnLCl}_2$  solutions of complexes **2b–2i** turned to a deep green color characteristic of Mn(III/IV) dimers. The stability of the green solutions varied significantly from species to species, but all of them precipitated  $\text{MnO}_2$  after long periods (>24 h) at room temperature. Complexes **1c** and **1d** (L = Cl-terpy and Br-terpy) are among the least stable in solution; the brown  $\text{MnO}_2$  precipitate was observed within 1 h even when the solutions were kept at 0 °C. To assign the green Mn complexes further, UV-vis spectroscopy, EPR spectroscopy, and ESI-MS studies of the in situ solutions were carried out.

Despite the differences between the ligands involved in the complexes, common UV-vis absorption features at 550 and around 650 nm (Figure 4) were observed in all eight cases that are indicative of in situ formation of the di- $\mu$ -oxo Mn(III/IV) dimers (**1b–1i**). These two features closely resemble the absorptions of the previously characterized  $[\text{Mn}^{\text{III/IV}}_2(\text{O})_2(\text{terpy})_2(\text{OH}_2)_2](\text{NO}_3)_3$  complex,<sup>7,32</sup> which were assigned to a d–d transition and an oxygen-to-manganese charge-transfer band, respectively, on the basis of the assignments of similar absorptions of  $[\text{Mn}^{\text{III/IV}}_2\text{O}_2(\text{bpy})_4]^{3+}$ .<sup>33</sup> Further addition of oxone oxidizes the Mn(III/IV) complexes to the corresponding Mn(IV/IV) complexes, as is evident from the increase of a new absorption shoulder in the range 420–450 nm (Figure 4). The similarity in the UV-vis absorption bands suggests that the high-valent Mn dimer complexes share similar structures.

The ESI-MS spectra of solutions of **1** show peaks from the  $[\text{Mn}^{\text{III/IV}}_2(\text{O})_2\text{L}_2]^{3+}$  core paired with the available counterions. For Mn(III/IV) dimer complexes prepared in situ,

(32) Collomb, M. N.; Deronzier, A.; Richardot, A.; Pecaut, J. *New J. Chem.* **1999**, 23, 351.

(33) Cooper, S. R.; Calvin, M. *J. Am. Chem. Soc.* **1977**, 99, 6623.



**Table 4.** Selected Angles and Distances for Complexes **2b**,<sup>16</sup> **2e**, **2g**, **2k**, **2n**,<sup>18</sup> **3**,<sup>16</sup> and **4**<sup>16</sup>

	<b>2b</b> (X = Cl)	<b>2e</b> (X = Cl)	<b>2g</b> (X = Cl) <sup>b</sup>	<b>2k</b> (X = Cl) <sup>c</sup>	<b>2n</b> (X = Cl)	<b>3</b> (X = Br)	<b>4</b> (X = I)
T (°C) <sup>a</sup>	25	−100	−100	23	25	25	25
X(1)–Mn–N(2) (deg)	104.6	115.8	109.7 (122.6)	114.0	105.9	122.0	122.8
X(2)–Mn–N(2) (deg)	144.2	129.2	128.6	133.2	141.1	122.0	122.8
X(1)–Mn–X(2) (deg)	111.2	115.0	121.6 (108.7)	112.8	112.9	116.1	114.3
X(1)–Mn (Å)	2.37	2.36	2.29 (2.36)	2.35	2.38	2.50	2.72
X(2)–Mn (Å)	2.35	2.36	2.36	2.33	2.34	2.50	2.72
N(2)–Mn (Å)	2.21	2.21	2.21	2.19	2.28	2.20	2.23

<sup>a</sup> T, temperature of data collection; deg, degree. <sup>b</sup> The bond angles and distances involving the disordered Cl(1)' in **2g** are included in parentheses. <sup>c</sup> Numbering scheme of nitrogen and halogen atoms in all complexes follows that of **2k** in Figure 2, so that the X(1)–Mn–N(2) angle is smaller than that of X(2)–Mn–N(2).

the most prominent high-mass peaks were always found at *m/z* values corresponding to  $[\text{Mn}^{\text{III/IV}}_2(\text{O})_2\text{L}_2\text{Cl}_2]^+$  and  $[\text{Mn}^{\text{III/IV}}_2(\text{O})_2\text{L}_2(\text{SO}_4)]^+$  (Figure 5), as expected because  $\text{Cl}^-$  and  $\text{SO}_4^{2-}$  are the most abundant counterions in solution. The two water ligands of **1** are probably lost during the desolvation process in the MS, as was found in the ESI-MS spectra of similar compounds.<sup>5,32</sup> The assignment of the MS peaks is constrained by the *m/z* values and isotope peak ratios. On the basis of this information, charge considerations of the assigned peaks require, in both of the MS peaks, the existence of two oxo groups, two ligand molecules, and Mn(III) and Mn(IV) ions. This provides strong evidence that  $[\text{Mn}^{\text{III/IV}}_2(\text{O})_2\text{L}_2\text{X}_2]^{3+}$  exists in solution (where X = a labile ligand such as water, chloride, or sulfate).

The EPR spectra of the in situ-generated green species show a 16-line EPR signal (Figure 6), which is characteristic of mixed-valence Mn(III/IV) dimer complexes. Although slightly different hyperfine splitting patterns were previously reported for the  $[\text{Mn}^{\text{III/IV}}_2(\text{O})_2(\text{dipic})_2(\text{OH}_2)_2]^-$  and  $[\text{Mn}^{\text{III/IV}}_2(\text{O})_2(\text{bpy})_4]^{3+}$  complexes,<sup>34,35</sup> the 16-line signals observed for the solutions of complexes **1b–1i** are almost exactly the same (Figure 6), with only small differences in the line width. The replacement of terpy by structurally similar ligands does not seem to significantly perturb the electronic structure of the Mn(III/IV) dimer, less so than the replacement of terpy by dipic or bpy. The UV–vis, EPR, and ESI-MS data suggest that di- $\mu$ -oxo Mn(III/IV) dimer complexes with similar structures were successfully synthesized in solution.

Following the same procedure, the oxidation of **2j**, **2k**, **2l**, and **2m** led to red solutions, while a brown  $\text{MnO}_2$  precipitate formed immediately after the oxidation of **2n**. Sixteen-line EPR signals of lower intensity were observed in the case of **2j**, **2k**, and **2l** (Figure 6), although ESI-MS peaks corresponding to Mn(III/IV) dimers were observed only in the case of **2j**. The oxidized solutions of **2l** and **2m** show significant  $\text{Mn}^{\text{II}}$  EPR signals, suggesting the reduction of high-valent Mn species. Ligand oxidation, electronic effects, or steric effects in the case of L = bbp could contribute to the failure of Mn(III/IV) dimer complex formation.

Overall, the in situ synthesis of di- $\mu$ -oxo dimanganese(III/IV) complexes from the corresponding  $\text{Mn}^{\text{II}}\text{LCl}_2$  complex is simple and, in most cases, gives a good yield of the desired

**Table 5.** Yields and  $\text{O}_2$ -Evolving Activities of Solutions of Pure and in Situ Formed  $[\text{Mn}^{\text{III/IV}}_2(\mu\text{-O})_2(\text{L})_2(\text{X})_2]^{3+}$  Complexes

ligand, L (Mn dimer) <sup>a</sup>	yield (%) <sup>b</sup>	$\text{O}_2$ evolution rate (% of control) <sup>c</sup>
<i>t</i> Bu <sub>3</sub> -terpy ( <b>1h</b> ) – in situ	97	18
Ph-terpy ( <b>1e</b> ) – pure solution	100	25
Ph-terpy ( <b>1e</b> ) – in situ	80	35
EtO-terpy ( <b>1i</b> ) – in situ	77	47
terpy ( <b>1b</b> ) – pure solution	100	100
terpy ( <b>1b</b> ) – in situ	75	141
mesityl-terpy ( <b>1g</b> ) – pure solution	100	25
mesityl-terpy ( <b>1g</b> ) – in situ	60	40
tolyl-terpy ( <b>1f</b> ) – in situ	47	44
Cl-terpy ( <b>1c</b> ) – in situ	14	14
py-phen ( <b>1j</b> ) – in situ	11	12
Me <sub>2</sub> N-terpy ( <b>1l</b> ) – in situ	8	–
dpya ( <b>1k</b> ) – in situ	3	21
HO-terpy ( <b>1m</b> ) – in situ	0	–

<sup>a</sup> The  $\text{MnLCl}_2$  complexes were used as precursor complexes to generate the corresponding Mn(III/IV) dimers in situ (see text). <sup>b</sup> Percentage yields are calculated from EPR peak heights by normalizing to the peak height obtained for a solution of pure **1g** in 1:3 acetonitrile–water, diluted with an equal volume of 0.1 M acetate buffer at pH 4.5 (see text). <sup>c</sup> Rates are normalized to that obtained for a solution of pure **1b** in 1:3 acetonitrile–water (see text).

complex. The yields (Table 5) were obtained by measuring peak heights of the EPR signals in reference to a solution of **1g** as a standard (see Experimental Section). This procedure gives a series of new complexes with structures similar to that of  $[\text{Mn}^{\text{III/IV}}_2(\text{O})_2(\text{terpy})_2(\text{OH}_2)_2]^{3+}$ . The preparation and characterization of this family of complexes expands the limited number of known cases in which labile coordination sites are available on a di- $\mu$ -oxo-bridged dimanganese complex and, more importantly, provides the basis for a fast-screening assay for catalytic  $\text{O}_2$ -evolution activity.

Measurements of  $\text{O}_2$ -evolving activity are provided in Table 5. The use of  $\text{Mn}^{\text{II}}\text{LCl}_2$  complexes as precursors ensures no excess of free ligand (except in the case of **2g** where it was found to be desirable) or free  $\text{Mn}^{2+}$ , and thus enables comparative analyses of catalytic activity. In measuring catalytic activity, the  $\text{Mn}^{\text{II}}\text{LCl}_2$  precursors were first mixed with a measured amount of oxone that is just sufficient to form the complexes **1** (see Experimental Section). After allowing time for the assembly of **1** from the Mn(II) precursors (as judged by the appearance of green color), an aliquot of the solution was added to the assay solution containing excess oxone and the  $\text{O}_2$ -evolving activity was measured. Overall, the in situ solutions show significant activity, making the in situ assay a promising approach. A comparison of activities of solutions of the pure complexes **1b**, **1e**, and **1g** with those of solutions of the in situ-generated

(34) Limburg, J.; Crabtree, R. H.; Brudvig, G. W. *Inorg. Chim. Acta* **2000**, 297, 301.

(35) Cooper, S. R.; Dismukes, G. C.; Klein, M. P.; Calvin, M. *J. Am. Chem. Soc.* **1978**, 100, 7248.



complexes obtained from **2b**, **2e**, and **2g**, respectively, shows that activities of the in situ solutions compare favorably with their corresponding pure dimer solutions. The higher activities observed for some of the in situ solutions may be ascribed to the differences in solution conditions between the authentic dimer solutions and the in situ-assembled dimer solutions due to the unavoidable presence of added oxone in the latter case.

**Isolation of  $[\text{Mn}^{\text{III/IV}}_2(\text{O})_2\text{L}_2(\text{H}_2\text{O})_2](\text{NO}_3)_3$ .** In contrast to the short time scale of a catalytic run (<30 min), the isolation and crystallization of Mn(III/IV) dimer complexes takes a much longer time. Excess ligand is, therefore, used to stabilize the Mn complexes in solution. To minimize degradation, a low concentration of Mn(III/IV) dimer complexes (1 mM) was synthesized at 0 °C and kept slightly below this temperature as acetonitrile was removed in situ. With a large excess of  $\text{NO}_3^-$  present, the removal of acetonitrile led to the precipitation of  $[\text{Mn}^{\text{III/IV}}_2(\text{O})_2\text{L}_2(\text{H}_2\text{O})_2](\text{NO}_3)_3$ . To avoid ligand precipitation caused by the instability of the Mn(III/IV) dimer complexes in pure water, the green precipitates were isolated by filtration before the complete removal of acetonitrile. Difficulty in controlling this step often led to limited yields. Following this procedure,  $[\text{Mn}^{\text{III/IV}}_2(\text{O})_2(\text{Ph-terpy})_2(\text{H}_2\text{O})_2](\text{NO}_3)_3$  and  $[\text{Mn}^{\text{III/IV}}_2(\text{O})_2(\text{mesityl-terpy})_2(\text{H}_2\text{O})_2](\text{NO}_3)_3$  were successfully isolated and characterized by elemental analysis, while similar green compounds with Cl-terpy and Br-terpy were isolated but could not be obtained in a pure form. The EPR and ESI-MS spectra of the four compounds in 1:1 water–acetonitrile showed the presence of  $[\text{Mn}^{\text{III/IV}}_2(\text{O})_2\text{L}_2\text{X}_2]$  species.

Like their corresponding in situ solutions, aqueous solutions of the above four compounds are not stable. Within minutes, the initial green solutions turn brown with the formation of brown or white precipitates, depending on the complex. With the 1:1 acetonitrile–water mixture, all four complexes are soluble, with a particularly noticeable increase in solubility for **1c**, **1d**, and **1e**, although none of the resulting four solutions are stable indefinitely. The hydrophobic substituent groups (Cl-, Br-, Ph-, and mesityl-) on terpy appear to increase the solubility of the corresponding Mn(III/IV) complexes in  $\text{CH}_3\text{CN}$  from that of **1b**, which is almost completely insoluble. Judging by the color of the dissolved solutions, complex **1g** is very soluble in acetonitrile, while the other three are only slightly soluble. The significantly higher solubility of **1g** in acetonitrile versus **1e** may be owing to the difference in stacking of molecules in crystal structure (vide infra). In contrast to the low stability of **1g** in the presence of water, a solution of **1g** in dry acetonitrile was stable for several days at room temperature without color change. The high solubility of **1g** in acetonitrile and the stability of the resulting solution affords the opportunity to study the Mn(III/IV) complexes in non-aqueous solutions. Previously, organic solubility of  $[\text{Mn}^{\text{III/IV}}_2(\mu\text{-O})_2(\text{terpy})_2(\text{H}_2\text{O})_2]^{3+}$  complexes could only be achieved by substituting the coordinated waters of **1b** with  $\text{CF}_3\text{COO}^-$ . The previously isolated  $[\text{Mn}^{\text{III/IV}}_2(\mu\text{-O})_2(\text{terpy})_2(\text{CF}_3\text{CO}_2)_2](\text{CF}_3\text{CO}_2)$  (**5a**) and  $[\text{Mn}^{\text{III/IV}}_2(\mu\text{-O})_2(\text{terpy})_2(\text{CF}_3\text{CO}_2)_2](\text{ClO}_4)$  (**5b**) complexes are soluble in acetonitrile, and the resulting solutions were studied by electrochemistry.<sup>36,37</sup>

Following the preparation procedures for  $[\text{Mn}^{\text{III/IV}}_2\text{O}_2\text{L}_2(\text{H}_2\text{O})_2](\text{NO}_3)_3$ , but with a larger excess of mesityl-terpy (20% excess), slow evaporation of the 1:1 acetonitrile–water solution led to a mixture of colorless mesityl-terpy and black-green crystals of **1g** suitable for X-ray crystallography. An ORTEP diagram of  $[\text{Mn}^{\text{III/IV}}_2\text{O}_2(\text{mesityl-terpy})_2(\text{H}_2\text{O})_2](\text{NO}_3)_3$  (**1g**) is shown in Figure 3. Like  $[\text{Mn}^{\text{III/IV}}_2\text{O}_2(\text{terpy})_2(\text{H}_2\text{O})_2](\text{NO}_3)_3$  (**1b**),<sup>7</sup> two aqua ligands can be found coordinated to both Mn ions of a Mn–di- $\mu$ -oxo–Mn core. The di- $\mu$ -oxo-bridged Mn–Mn distance in **1g** (2.72 Å) is almost the same as that in **1b** (2.73 Å) and in other di- $\mu$ -oxo-bridged Mn dimers.<sup>3</sup> In **1g**, the dihedral angle between the central pyridine ring and its aromatic pendant is 71.0°, similar to that of the free ligand (67.5°)<sup>31</sup> and Mn(mesityl-terpy) $\text{Cl}_2$  (74.8°). As in the case of **2g**, the sterically demanding mesityl groups in **1g** may prevent close packing of the molecules, leading to smaller  $d_{\text{cal}}$  (1.461 g/cm<sup>3</sup>, compared to  $d_{\text{cal}}$  = 1.614 g/cm<sup>3</sup> of **1b**), and may contribute to the enhanced solubility of **1g** in acetonitrile compared to that of **1b** and **1e**.

One major difference between the structures of **1b**, **1g**, and **5b** is that the two Mn ions of **1b** are crystallographically equivalent, while those of **5b** and **1g** are inequivalent. The Mn(1) of **1g** is typical of an axially elongated d<sup>4</sup> Mn(III) ion in that the Mn(1)–N<sub>ax</sub> distances (Mn(1)–N(1), 2.22 Å and Mn(1)–N(3), 2.19 Å) are significantly longer than the Mn(1)–N<sub>eq</sub> distance (2.05 Å). In contrast, the Mn(2)–N<sub>ax</sub> distances (Mn(2)–N(4), 2.06 Å and Mn(2)–N(6), 2.04 Å) are almost the same as the Mn(2)–N<sub>eq</sub> distance (2.04 Å), suggesting that Mn(2) is a normal d<sup>3</sup> Mn(IV) ion. All Mn–O and Mn–N distances of Mn(2) are shorter than the corresponding bond distances of Mn(1); this confirms the assignment of Mn(1) as higher-valent Mn(IV). The inequivalency of the two Mn ions in **1g** is consistent with its 16-line EPR signal, which is the result of hyperfine coupling between an  $S = 1/2$  electron spin with two inequivalent <sup>55</sup>Mn nuclei.

The different equivalency of the Mn ions in **1b** versus **1g** and **5b** is reminiscent of the known disorder phenomena in the phen/bpy Mn(III/IV) dimers. The Mn ions are crystallographically inequivalent in  $[\text{Mn}^{\text{III/IV}}_2\text{O}_2(\text{bpy})_4](\text{ClO}_4)_3$  (**6a**) and  $[\text{Mn}^{\text{III/IV}}_2\text{O}_2(\text{phen})_4](\text{ClO}_4)_3$  (**6b**) but are equivalent in  $[\text{Mn}^{\text{III/IV}}_2\text{O}_2(\text{bpy})_4](\text{PF}_6)_3$  (**6c**).<sup>38–40</sup> On the basis of EPR studies and the analysis of thermal displacement parameters of **6c**, the crystallographic equivalency of the Mn ions in **6c** has been concluded to be the result of disorder of inequivalent Mn<sup>III</sup> and Mn<sup>IV</sup> ions.<sup>38,39</sup> In light of these previous results,

The different equivalency of the Mn ions in **1b** versus **1g** and **5b** is reminiscent of the known disorder phenomena in the phen/bpy Mn(III/IV) dimers. The Mn ions are crystallographically inequivalent in  $[\text{Mn}^{\text{III/IV}}_2\text{O}_2(\text{bpy})_4](\text{ClO}_4)_3$  (**6a**) and  $[\text{Mn}^{\text{III/IV}}_2\text{O}_2(\text{phen})_4](\text{ClO}_4)_3$  (**6b**) but are equivalent in  $[\text{Mn}^{\text{III/IV}}_2\text{O}_2(\text{bpy})_4](\text{PF}_6)_3$  (**6c**).<sup>38–40</sup> On the basis of EPR studies and the analysis of thermal displacement parameters of **6c**, the crystallographic equivalency of the Mn ions in **6c** has been concluded to be the result of disorder of inequivalent Mn<sup>III</sup> and Mn<sup>IV</sup> ions.<sup>38,39</sup> In light of these previous results,

(36) Baffert, C.; Collomb, M. N.; Deronzier, A.; Pecaut, J.; Limburg, J.; Crabtree, R. H.; Brudvig, G. W. *Inorg. Chem.* **2002**, *41*, 1404.

(37) Baffert, C.; Chen, H. Y.; Crabtree, R. H.; Brudvig, G. W.; Collomb, M. N. *J. Electroanal. Chem.* **2001**, *506*, 99.

(38) Manchanda, R.; Brudvig, G. W.; Degala, S.; Crabtree, R. H. *Inorg. Chem.* **1994**, *33*, 5157.

(39) Stebler, M.; Ludi, A.; Burgi, H. B. *Inorg. Chem.* **1986**, *25*, 4743.

(40) Plaksin, P. M.; Palenik, G. J.; Stouffer, R. C.; Mathew, M. *J. Am. Chem. Soc.* **1972**, *94*, 2121.

it is likely that the equivalency of Mn ions in **1b** is also due to disorder of Mn<sup>III</sup> and Mn<sup>IV</sup> ions.

## Conclusion

In this study, we reported the general in situ synthesis of [Mn<sup>III/IV</sup><sub>2</sub>(O)<sub>2</sub>(L)<sub>2</sub>(X)<sub>2</sub>]<sup>3+</sup> (**1**) complexes from Mn<sup>II</sup>LCl<sub>2</sub> (**2**) precursors. Complexes **1** were generated and characterized by UV–vis, EPR, ESI-MS and oxygen-evolving activity assays. The yields and oxygen-evolving activities were found to vary greatly depending on the particular complex. The reasons are currently under investigation.

The preparation of this family of complexes has expanded the limited number of known di- $\mu$ -oxo-bridged manganese complexes that contain labile coordination sites that could be transiently occupied by water in aqueous solution. This type of complex is of importance because water is the substrate of the oxygen-evolving complex of photosystem II, where Mn–di- $\mu$ -oxo–Mn moieties are known to be part of the active catalyst.<sup>2</sup> In studies where synthetic compounds were used to model this enzymatic process, water coordination on Mn was found to be the key element in successful catalysts.<sup>7,11,12</sup> Our simple in situ preparation of **1** enables a fast-screening procedure for a catalytic assay for O<sub>2</sub> evolution. The use of Mn<sup>II</sup>LCl<sub>2</sub> complexes as precursors is advantageous, as it minimizes the presence of organic impurities, excess ligand, or free Mn<sup>2+</sup> in the catalytic

solution. The oxidation of any of these species may lead to undesired pathways. The current ligand library covers a range of ligands with different electron-donating/withdrawing ability as well as ligands that restrict the rotation of the pyridine rings of terpy (py-phen and dpva).

Crystals of Mn<sup>II</sup>(dpva)Cl<sub>2</sub>, Mn<sup>II</sup>(Ph-terpy)Cl<sub>2</sub>, Mn<sup>II</sup>(mesityl-terpy)Cl<sub>2</sub>, and [Mn<sup>III/IV</sup><sub>2</sub>(O)<sub>2</sub>(mesityl-terpy)<sub>2</sub>(H<sub>2</sub>O)<sub>2</sub>](NO<sub>3</sub>)<sub>3</sub> (**1g**) were isolated and characterized by X-ray crystallography. As in **5b**, the two Mn ions in **1g** are crystallographically inequivalent; this provides structural evidence that the di- $\mu$ -oxo-bridged Mn(III/IV) dimers are valence-trapped. Complex **1g** is a di- $\mu$ -oxo di-aqua dimanganese complex that has good solubility in an organic solvent (acetonitrile); this will enable further studies in acetonitrile where the concentration of water can be varied.

**Acknowledgment.** The authors thank the National Institutes of Health (GM32715) and the U.S. Department of Energy (DE-FG02-84ER13297) for financial support and Marie-Noëlle Collomb for communicating results prior to publication and for helpful discussions.

**Supporting Information Available:** X-ray crystallographic data of **2e**, **2g**, **2k**, and **1g** (pdf); X-ray crystallographic file for **2e**, **2g**, **2k**, and **1g** (cif). This material is available free of charge via the Internet at <http://pubs.acs.org>.

IC0509940